

pubs.acs.org/JACS Communication

Manipulating Atomic Structures at the Au/TiO₂ Interface for O₂ Activation

Jiawei Huang, Shuai He, Justin L. Goodsell, Justin R. Mulcahy, Wenxiao Guo, Alexander Angerhofer, and Wei David Wei*



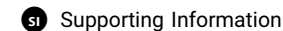
Cite This: J. Am. Chem. Soc. 2020, 142, 6456–6460



ACCESS

Metrics & More





ABSTRACT: The metal/oxide interface has been extensively studied due to its importance for heterogeneous catalysis. However, the exact role of interfacial atomic structures in governing catalytic processes still remains elusive. Herein, we demonstrate how the manipulation of atomic structures at the Au/TiO₂ interface significantly alters the interfacial electron distribution and prompts O₂ activation. It is discovered that at the defect-free Au/TiO₂ interface electrons transfer from Ti³⁺ species into Au nanoparticles (NPs) and further migrate into adsorbed perimeter O₂ molecules (i.e., in the form of Au–O–O–Ti), facilitating O₂ activation and leading to a ca. 34 times higher CO oxidation activity than that on the oxygen vacancy (V_o)-rich Au/TiO₂ interface, at which electrons from Ti³⁺ species are trapped by interfacial V_o on TiO₂ and hardly interact with perimeter O₂ molecules. We further reveal that the calcination releases those trapped electrons from interfacial V_o to facilitate O₂ activation. Collectively, our results establish an atomic-level description of the underlying mechanism regulating metal/oxide interfaces for the optimization of heterogeneous catalysis.

he integration of metal nanoparticles (NPs) with oxides offers unique opportunities for driving catalytic reactions as compared to their catalytically inaccessible single-component counterparts. ¹⁻¹⁶ However, an understanding of the exact functionality of atomic structures at metal/oxide interfaces in governing the catalytic activity and its implications for practical applications has not yet been established. 17,18 For instance, interfacial atomic structures of Au/TiO2 heterostructures are complicated when Au is nucleated at surface defects with various coordinated structures of different facets, surface structures, and grain boundaries of TiO₂ NPs. 19-21 Another major limitation is the lack of strategies for constructing distinct atomic structures solely at the metal/ oxide interface rather than adjusting atomic and electronic structures of whole oxides, 22,23 making it challenging to correlate the interfacial-structure-dependent electron distribution with the catalytic activity.

In this contribution, we reported how interfacial atomic structures of metal/oxide were manipulated to alter the electron distribution and promote O2 activation for CO oxidation. Using different fabrication strategies, we successfully fabricated two Au/TiO2 heterostructures with distinct interfaces and revealed that for the defect-free Au/TiO2 interface electrons originated from Ti3+ species were transferred from TiO2 into Au NPs, while those electrons were trapped at V_o on TiO₂ at the V_o-rich interface. Further investigations showed that such divergent electron distributions on Au/TiO₂ heterostructures resulted in significantly different efficiencies for electron-driven O2 activation. For Au/ TiO₂ with the defect-free interface, electrons that transferred from Ti³⁺ species into Au NPs further migrated to O₂ molecules adsorbed on the perimeter (i.e., in the form of Au-O-O-Ti) to promote O₂ activation. This led to a ca. 34 times higher CO oxidation than that on Au/TiO₂ with the V_o - rich interface, where electrons were mainly trapped at interfacial $V_{\rm o}$ on ${\rm TiO_2}$ and were inhibited from interacting with perimeter ${\rm O_2}$ molecules. Moreover, we discovered that calcination at 320 °C significantly decreased the amount of $V_{\rm o}$ at the $V_{\rm o}$ -rich ${\rm Au/TiO_2}$ interface, releasing electrons initially trapped at the interfacial $V_{\rm o}$ on ${\rm TiO_2}$ for improving the efficiency of ${\rm O_2}$ activation.

Two Au/TiO₂ heterostructures, with a defect-free interface or V_0 -rich interface, were prepared (Figure 1A and B). Using the deposition-precipitation (DP) method, 24 chloroauric acid trihydrate (HAuCl₄·3H₂O) was directly reduced on the surface of TiO₂ NPs. The diffusion of Au atoms into surface V_0 on TiO₂ mediated the formation of chemical bonds with Ti atoms²² and developed a defect-free interface (Figure S1A). Meanwhile, through a modified colloidal-deposition (CD) method,²⁵ presynthesized Au NPs were directly deposited onto TiO₂ NPs, maintaining V_o at the Au/TiO₂ interface (Figure S1B). X-ray photoelectron spectroscopy (XPS) proved that no observable citrate ions remained on Au NPs in Au/TiO2 heterostructures with the V_0 -rich interface (Figure S2A). It is noted that with the exception of different atomic structures, both defect-free and V_o-rich Au/TiO₂ interfaces contained well-defined nanoscale physical contacts to ensure the interfacial electron transfer (Figure 1C and D). 24,26,27

When compared to Au/SiO₂ heterostructures (i.e., 84.0 \pm 0.1 eV in Figure S2B), high-resolution XPS showed that the Au

Received: December 13, 2019 Published: March 23, 2020





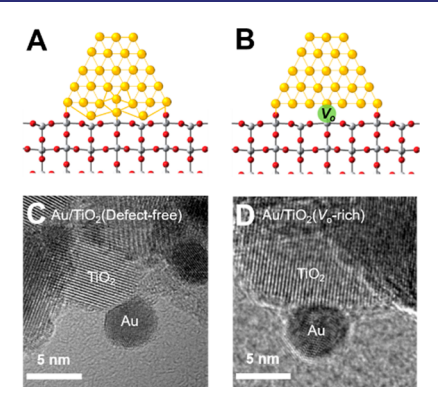


Figure 1. Au/TiO $_2$ heterostructures with distinct interfaces. Schematic of Au/TiO $_2$ heterostructures with (A) the defect-free interface and (B) the V_o -rich interface. The yellow, red, and silver dots represent gold, oxygen, and titanium atoms, respectively. The green dot stands for the interfacial V_o . High-resolution transmission electron microscopy (HRTEM) images of Au/TiO $_2$ heterostructures with (C) the defect-free interface and (D) the V_o -rich interface.

 $4f_{7/2}$ of both Au/TiO₂ heterostructures shifted to the lower binding energies (Figure 2A: 83.6 \pm 0.1 eV for the defect-free

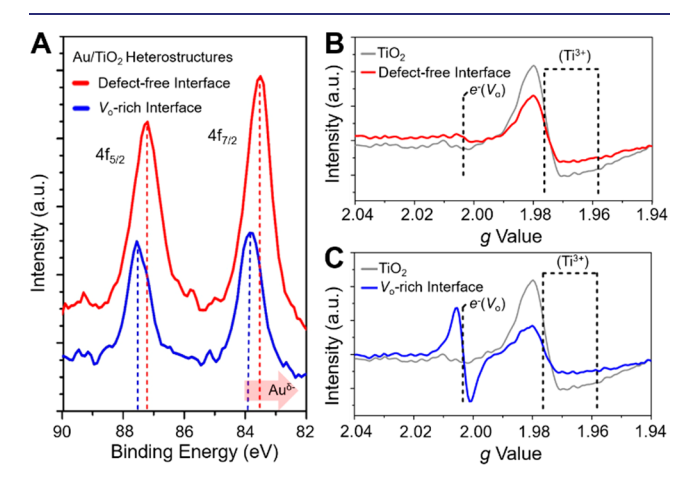


Figure 2. Electron distributions on Au/TiO₂ heterostructures with distinct interfaces. (A) High-resolution XPS spectra of the Au 4f orbital for Au/TiO2 heterostructures with the defect-free interface (red curve) and Au/TiO₂ heterostructures with the V₀-rich interface (blue curve). Note: The energy resolution of XPS spectra is 0.1 eV. Different intensities of Au 4f spectra might come from the nonuniform distribution of Au/TiO2 heterostructures on the Si wafer during the XPS sample preparation. (B) X-band EPR spectra of bare TiO2 NPs (gray curve) and Au/TiO2 heterostructures with the defect-free interface (red curve) at 90 K. (C) X-band EPR spectra of bare TiO2 NPs (gray curve) and Au/TiO2 heterostructures with the V_0 -rich interface (blue curve) at 90 K. Note: EPR comparisons between bare TiO2 and two Au/TiO2 heterostructures were carried out using the same amount of samples (ca. 40 \pm 2 mg). $e^{-}(V_0)$ represents electrons trapped at Vo on TiO2, and Ti3+ stands for electrons accumulated at Ti centers of rutile TiO2. The EPR background spectrum has been subtracted from the initial spectra of TiO₂ and two Au/TiO₂ heterostructures.

interface and 83.8 \pm 0.1 eV for the $V_{\rm o}$ -rich interface). This indicated that electrons transferred from TiO₂ into Au NPs via the heterogeneous interface. Moreover, the lower binding energy of Au $4f_{7/2}$ (i.e., 83.6 \pm 0.1 eV) strongly suggested that more electrons were transferred from TiO₂ to Au for Au/TiO₂ heterostructures with the defect-free interface.

Distinct electron distributions between those two Au/TiO₂ heterostructures were further verified using X-band electron paramagnetic resonance (EPR) spectroscopy. Compared to bare TiO2 NPs, the EPR feature of electrons accumulated at Ti centers (i.e., Ti³⁺ species)²⁸⁻³⁰ significantly decreased on Au/ TiO₂ heterostructures with the defect-free interface (Figure 2B and Figure S3A and B), suggesting that electrons transferred from Ti³⁺ species of TiO₂ into Au NPs (i.e., EPR silent) (Figure S4A). Additionally, no V_o -related EPR feature was observed at the defect-free Au/TiO2 interface even with 5 wt % Au (Figure S5), demonstrating that the addition of Au NPs on TiO_2 did not affect the distribution of V_0 in TiO_2 to influence the electron distribution at the defect-free Au/TiO₂ interface. For Au/TiO₂ heterostructures with the V_0 -rich interface, despite the observation of a similar decrease of Ti³⁺ species, a new EPR feature (g = 2.003) appeared and was assigned to electrons trapped at V_0 of TiO₂ (Figure 2C, blue curve, and Figure S3C). ^{28–30} Interestingly, the intensity of this EPR feature continued to rise when the Au NP loading was increased (Figure S6), confirming that those V_0 must be placed exactly at the Au/TiO2 interface. Thus, electrons originally from Ti^{3+} species would be trapped at the interfacial V_0 of TiO₂ rather than transferring into Au NPs (Figure S4B).

The electron distribution at the Au/TiO₂ interface has been reported to determine the activation of perimeter O₂ molecules, in which negatively charged Au NPs induced by the interfacial electron transfer from ${\rm TiO_2}$ to Au exhibit a higher O₂ activation efficiency than that on neutral Au NPs. S,31,32 Meanwhile, it is known that the vibrational mode of adsorbed carbon monoxide molecules $\nu({\rm CO})$ is sensitive to the change of electron density of Au NPs, Making CO an ideal molecular probe to spectroscopically study the electron-distribution-dependent O₂ activation on those two Au/TiO₂ heterostructures *in operando*.

For Au/TiO₂ heterostructures with the defect-free interface, two vibrational signatures were observed during O2 activation (Figure 3A) that were distinct from the mode observed for adsorbed CO before O_2 activation (i.e., $2103 \pm 2 \text{ cm}^{-1}$ in Figure S7A and B). Interestingly, both CO vibrational modes blue-shifted $(\nu_1(CO)_{O_2} = 2130 \pm 2 \text{ cm}^{-1} \text{ and } \nu_2(CO)_{O_2} =$ $2118 \pm 2 \text{ cm}^{-1}$), suggesting a decrease of electron density on Au NPs during O2 activation as the reduced electron density on Au weakened the Au-CO π-back-bonding. 33,35 Furthermore, density functional theory (DFT) calculations found that during O2 activation interfacial Au atoms near perimeter O2 molecules were more electron-deficient than those away from the interface (Figure S8). Accordingly, we assigned $\nu_1(CO)_{O_2}$ to CO molecules adsorbed at the Au/TiO2 perimeter and $\nu_2(CO)_{O_2}$ to CO molecules adsorbed on Au atoms away from the interface (Figure 3B). DFT calculations confirmed that once the electron density on Au NPs decreased, perimeter O₂ molecules became negatively charged (Figure S8), suggesting that electrons were transferred from Au NPs into perimeter O₂ molecules for O_2 activation (Figure 3B).

Vibrational modes of adsorbed CO molecules on Au/TiO₂ heterostructures with the $V_{\rm o}$ -rich interface ($\nu_1({\rm CO})_{{\rm O}_2}$ = 2128 \pm 2 cm⁻¹ and $\nu_2({\rm CO})_{{\rm O}_2}$ = 2116 \pm 2 cm⁻¹ in Figure 3C) were also found to blue-shift during O₂ activation compared to signals observed before O₂ activation (i.e., 2107 \pm 2 cm⁻¹ in Figure S7C and D). However, blue-shifts of both vibrational modes were less than those on Au/TiO₂ heterostructures with

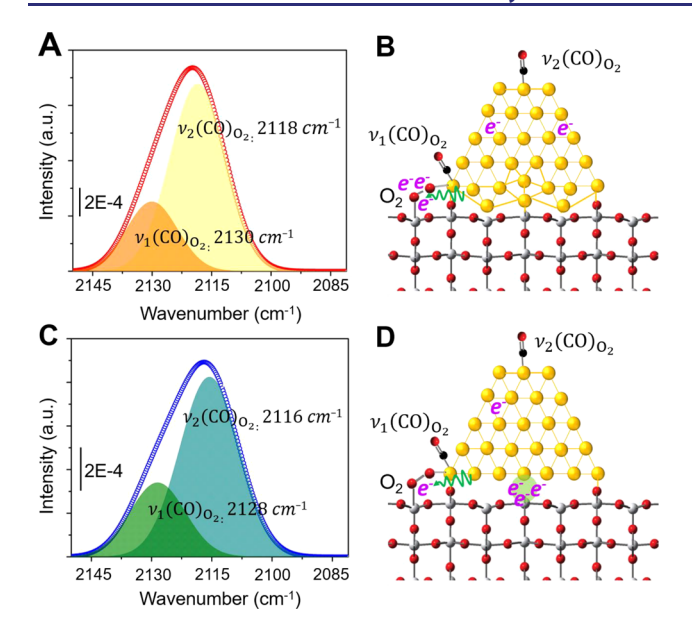


Figure 3. In operando diffuse reflectance infrared Fourier transform spectroscopy (DRIFTS) for O2 activation on Au/TiO2 heterostructures with distinct interfaces. (A) In operando DRIFTS spectra of $\nu(CO)$ during O_2 activation on Au/Ti O_2 heterostructures with the defect-free interface. $\nu_1({\rm CO})_{{\rm O}_2}$ and $\nu_2({\rm CO})_{{\rm O}_2}$ were observed at 2130 and 2118 cm⁻¹, respectively. (B) Schematic of O₂ activation on the defect-free Au/TiO2 interface. The electron transfer from Au NPs into perimeter O2 molecules resulted in less electron density within the interfacial Au-CO region than that of the area located away from the interface. (C) In operando DRIFTS spectra of ν (CO) during O₂ activation on $\mathrm{Au/TiO_2}$ heterostructures with the V_o -rich interface. $\nu_1(\text{CO})_{\text{O}_2}$ and $\nu_2(\text{CO})_{\text{O}_2}$ were observed at 2128 and 2116 cm⁻¹, respectively. (D) Schematic of O₂ activation on the V₀-rich Au/TiO₂ interface. The interfacial V_0 trapped electrons and hindered the electron-driven O2 activation, suppressing interfacial CO oxidation. Note: the resolution of DRIFTS spectra is 2 cm⁻¹, and CO molecules detected in the headspace have been removed from the spectra. Since DRIFTS spectra were collected during the O2 activation, surfaceadsorbed CO molecules kept being oxidized by perimeter O2 molecules, resulting in weak CO vibrational signals.

the defect-free interface, suggesting that fewer electrons were transferred from Au NPs into perimeter O_2 molecules on the $V_{\rm o}$ -rich Au/Ti O_2 interface. Further DFT calculations showed less of a decrease of electron density on the Au surface (Figure S9). This observation is consistent with that demonstrated in our XPS and EPR measurements of Au/Ti O_2 heterostructures with the $V_{\rm o}$ -rich interface (Figure 2A and C): electrons were trapped at the interfacial $V_{\rm o}$ and, consequently, were hardly transferred into perimeter O_2 molecules (Figure 3D).

Different amounts of interfacial electrons transferred into perimeter O_2 molecules on these two Au/TiO_2 heterostructures led to discrete efficiencies for O_2 activation, which is the rate-determining step in CO oxidation. ^{6,36,37} As shown in Figure S10A, the activation barrier of CO oxidation on Au/TiO_2 heterostructures with the defect-free interface (12.6 \pm 1.9 kJ/mol) was much smaller than that on Au/TiO_2 heterostructures with the V_0 -rich interface (34.6 \pm 2.7 kJ/mol). This result confirmed that more electrons migrated from Au into perimeter O_2 molecules on the defect-free interface and significantly facilitated O_2 activation, eventually leading to a ca. 34 times higher activity of CO oxidation than that on Au/V

 ${
m TiO_2}$ heterostructures with the $V_{
m o}$ -rich interface (Figure S10B).

High-temperature calcination has been used to reconstruct interfacial atomic structures between metal NPs and oxides. Signare S11 showed that, after treating Au/TiO₂ heterostructures with the $V_{\rm o}$ -rich interface at 320 °C for 3 h, calcination significantly decreased the amount of interfacial $V_{\rm o}$, suggesting that electrons were released from interfacial $V_{\rm o}$ into perimeter O₂ molecules to promote O₂ activation for CO oxidation. Indeed, we observed a ca. 18.5 times higher activity of CO oxidation after the calcination (Figure S12).

In summary, we have successfully manipulated atomic structures at the Au/TiO2 interface to alter the interfacial electron distribution and promote the catalytic activity. Compared to the V_0 -rich interface, Au/TiO₂ heterostructures with the defect-free interface showed significantly higher efficiency for O2 activation. Spectroscopic studies revealed that the defect-free interface permitted the electron transfer from TiO₂ into Au NPs to activate adsorbed perimeter O₂ molecules. By contrast, the V_0 -rich interface trapped electrons at V_0 on TiO₂ and prevented electrons from interacting with perimeter O2 molecules. Moreover, we found that calcination significantly decreased the amount of interfacial V_0 at the V_0 rich Au/TiO2 interface and released electrons from interfacial V_0 to promote O_2 activation, further illustrating the importance of manipulating interfacial atomic structures in facilitating heterogeneous catalysis. Taken together, our results not only establish an atomic-level understanding of the interfacialstructure-dependent catalytic activity on Au/TiO2 heterostructures but also provide strategies to engineer metal/oxide interfaces for optimizing heterogeneous catalysis.

ASSOCIATED CONTENT

Supporting Information

The Supporting Information is available free of charge at https://pubs.acs.org/doi/10.1021/jacs.9b13453.

Experimental details and additional data (PDF)

AUTHOR INFORMATION

Corresponding Author

Wei David Wei — Department of Chemistry and Center for Catalysis, University of Florida, Gainesville, Florida 32611, United States; orcid.org/0000-0002-3121-5798; Email: wei@chem.ufl.edu

Authors

Jiawei Huang — Department of Chemistry and Center for Catalysis, University of Florida, Gainesville, Florida 32611, United States; Occid.org/0000-0002-5184-2510

Shuai He – Department of Chemistry and Center for Catalysis, University of Florida, Gainesville, Florida 32611, United States Justin L. Goodsell – Department of Chemistry and Center for Catalysis, University of Florida, Gainesville, Florida 32611,

Justin R. Mulcahy – Department of Chemistry and Center for Catalysis, University of Florida, Gainesville, Florida 32611, United States

Wenxiao Guo — Department of Chemistry and Center for Catalysis, University of Florida, Gainesville, Florida 32611, United States; ocid.org/0000-0002-6674-9714

Alexander Angerhofer — Department of Chemistry and Center for Catalysis, University of Florida, Gainesville, Florida 32611, United States; orcid.org/0000-0002-8580-6024

Complete contact information is available at: https://pubs.acs.org/10.1021/jacs.9b13453

Notes

The authors declare no competing financial interest.

ACKNOWLEDGMENTS

This work is supported by the National Science Foundation under Grants CHE-1808539 and DMR-1352328. Materials characterization was conducted at MAIC and NRF, College of Engineering Research Service Centers, University of Florida. XPS characterization was conducted using an instrument purchased with NSF grant MRI-DMR-1126115. Computational supports were provided by HiPerGator 2.0, University of Florida Research Computing. W.G. especially appreciates the support of a graduate school fellowship from the University of Florida and the Department of Energy (DOE) Science Graduate Student Research (SCGSR) award.

REFERENCES

- (1) Haruta, M.; Tsubota, S.; Kobayashi, T.; Kageyama, H.; Genet, M. J.; Delmon, B. Low-temperature oxidation of CO over gold supported on TiO_2 , α -Fe₂O₃, and Co_3O_4 . *J. Catal.* **1993**, *144*, 175–192.
- (2) Schubert, M. M.; Hackenberg, S.; Van Veen, A. C.; Muhler, M.; Plzak, V.; Behm, J. J. CO oxidation over supported gold catalysts "Inert" and 'active' support materials and their role for the oxygen supply during reaction. *J. Catal.* **2001**, *197*, 113–122.
- (3) Chen, M.; Goodman, D. W. Catalytically active gold: From nanoparticles to ultrathin films. *Acc. Chem. Res.* **2006**, *39*, 739–746.
- (4) Cargnello, M.; Doan-Nguyen, V. V. T.; Gordon, T. R.; Diaz, R. E.; Stach, E. A.; Gorte, R. J.; Fornasiero, P.; Murray, C. B. Control of Metal Nanocrystal Size Reveals Metal-Support Interface Role for Ceria Catalysts. *Science* **2013**, *341*, 771–774.
- (5) Min, B. K.; Friend, C. M. Heterogeneous gold-based catalysis for green chemistry: Low-temperature CO oxidation and propene oxidation. *Chem. Rev.* **2007**, *107*, 2709–2724.
- (6) Green, I. X.; Tang, W.; Neurock, M.; Yates, J. T. Insights into catalytic oxidation at the Au/TiO_2 dual perimeter sites. *Acc. Chem. Res.* **2014**, 47, 805–815.
- (7) Chen, M.; Cai, Y.; Yan, Z.; Goodman, D. W. On the origin of the unique properties of supported Au nanoparticles. *J. Am. Chem. Soc.* **2006**, 128, 6341–6346.
- (8) Goodman, M. S. C. D. W. The Structure of Catalytically Active Gold on Titania. *Science* **2004**, *306*, 252–255.
- (9) Vajda, S.; White, M. G. Catalysis Applications of Size-Selected Cluster Deposition. *ACS Catal.* **2015**, *5*, 7152–7176.
- (10) DeRita, L.; Resasco, J.; Dai, S.; Boubnov, A.; Thang, H. V.; Hoffman, A. S.; Ro, I.; Graham, G. W.; Bare, S. R.; Pacchioni, G.; Pan, X.; Christopher, P. Structural evolution of atomically dispersed Pt catalysts dictates reactivity. *Nat. Mater.* **2019**, *18*, 746–751.
- (11) Hemmingson, S. L.; Campbell, C. T. Trends in Adhesion Energies of Metal Nanoparticles on Oxide Surfaces: Understanding Support Effects in Catalysis and Nanotechnology. ACS Nano 2017, 11, 1196–1203.
- (12) Li, D.; Chen, S.; You, R.; Liu, Y.; Yang, M.; Cao, T.; Qian, K.; Zhang, Z.; Tian, J.; Huang, W. Titania-morphology-dependent dual-perimeter-sites catalysis by Au/TiO₂ catalysts in low-temperature CO oxidation. *J. Catal.* **2018**, *368*, 163–171.
- (13) Li, X.; Yang, X.; Huang, Y.; Zhang, T.; Liu, B. Supported Noble-Metal Single Atoms for Heterogeneous Catalysis. *Adv. Mater.* **2019**, *31*, 1902031.

- (14) Liu, L.; Corma, A. Metal Catalysts for Heterogeneous Catalysis: From Single Atoms to Nanoclusters and Nanoparticles. *Chem. Rev.* **2018**, *118*, 4981–5079.
- (15) Polo-Garzon, F.; Fung, V.; Nguyen, L.; Tang, Y.; Tao, F.; Cheng, Y.; Daemen, L. L.; Ramirez-Cuesta, A. J.; Foo, G. S.; Zhu, M.; Wachs, I. E.; Jiang, D.; Wu, Z. Elucidation of the Reaction Mechanism for High-Temperature Water Gas Shift over an Industrial-Type Copper-Chromium-Iron Oxide Catalyst. *J. Am. Chem. Soc.* **2019**, *141*, 7990–7999.
- (16) Zhao, N.; He, C.; Liu, J.; Gong, H.; An, T.; Xu, H.; Zhao, F.; Hu, R.; Ma, H.; Zhang, J. Dependence of catalytic properties of Al/Fe₂O₃ thermites on morphology of Fe₂O₃ particles in combustion reactions. *J. Solid State Chem.* **2014**, 219, 67–73.
- (17) Kumar, G.; Tibbitts, L.; Newell, J.; Panthi, B.; Mukhopadhyay, A.; Rioux, R. M.; Pursell, C. J.; Janik, M.; Chandler, B. D. Evaluating differences in the active-site electronics of supported Au nanoparticle catalysts using Hammett and DFT studies. *Nat. Chem.* **2018**, *10*, 268–274.
- (18) Chen, A.; Yu, X.; Zhou, Y.; Miao, S.; Li, Y.; Kuld, S.; Sehested, J.; Liu, J.; Aoki, T.; Hong, S.; Camellone, M. F.; Fabris, S.; Ning, J.; Jin, C.; Yang, C.; Nefedov, A.; Wöll, C.; Wang, Y.; Shen, W. Structure of the catalytically active copper-ceria interfacial perimeter. *Nat. Catal.* **2019**, *2*, 334–341.
- (19) Thompson, T. L.; Yates, J. T. Surface science studies of the photoactivation of TiO₂ New photochemical processes. *Chem. Rev.* **2006**, *106*, 4428–4453.
- (20) Diebold, U. The surface science of titanium dioxide. *Surf. Sci. Rep.* **2003**, 48, 53–229.
- (21) Tsukamoto, D.; Shiraishi, Y.; Sugano, Y.; Ichikawa, S.; Tanaka, S.; Hirai, T. Gold nanoparticles located at the interface of anatase/rutile TiO₂ particles as active plasmonic photocatalysts for aerobic oxidation. *J. Am. Chem. Soc.* **2012**, *134*, 6309–6315.
- (22) Matthey, D.; Wang, J. G.; Wendt, S.; Matthiesen, J.; Schaub, R.; Lægsgaard, E.; Hammer, B.; Besenbacher, F. Enhanced Bonding of Gold Nanoparticles on Oxidized TiO₂(110). *Science* **2007**, *315*, 1692.
- (23) Wang, Y.; Widmann, D.; Behm, R. J. Influence of TiO₂ Bulk Defects on CO Adsorption and CO Oxidation on Au/TiO₂: Electronic Metal-Support Interactions (EMSIs) in Supported Au Catalysts. ACS Catal. 2017, 7, 2339–2345.
- (24) Qian, K.; Sweeny, B. C.; Johnston-Peck, A. C.; Niu, W.; Graham, J. O.; Duchene, J. S.; Qiu, J.; Wang, Y.; Engelhard, M. H.; Su, D.; Stach, E. A.; Wei, D. W. Surface plasmon-driven water reduction: Gold nanoparticle size matters. *J. Am. Chem. Soc.* **2014**, *136*, 9842–9845.
- (25) Tanaka, A.; Ogino, A.; Iwaki, M.; Hashimoto, K.; Ohnuma, A.; Amano, F.; Ohtani, B.; Kominam, H. Gold-Titanium(IV) Oxide Plasmonic Photocatalysts Prepared by a Colloid-Photodeposition Method: Correlation Between Physical Properties and Photocatalytic Activities. *Langmuir* 2012, 28, 13105–13111.
- (26) Duchene, J. S.; Sweeny, B. C.; Johnston-Peck, A. C.; Su, D.; Stach, E. A.; Wei, W. D. Prolonged hot electron dynamics in plasmonic-metal/semiconductor heterostructures with implications for solar photocatalysis. *Angew. Chem., Int. Ed.* **2014**, 53, 7887–7891.
- (27) He, S.; Huang, J.; Goodsell, J. L.; Angerhofer, A.; Wei, W. D. Plasmonic Nickel-TiO₂ Heterostructures for Visible-Light-Driven Photochemical Reactions. *Angew. Chem., Int. Ed.* **2019**, 58, 1–5.
- (28) Priebe, J. B.; Radnik, J.; Lennox, A. J. J.; Pohl, M. M.; Karnahl, M.; Hollmann, D.; Grabow, K.; Bentrup, U.; Junge, H.; Beller, M.; Brückner, A. Solar Hydrogen Production by Plasmonic Au-TiO₂ Catalysts: Impact of Synthesis Protocol and TiO₂ Phase on Charge Transfer Efficiency and H₂ Evolution Rates. *ACS Catal.* **2015**, *S*, 2137–2148.
- (29) Priebe, J. B.; Karnahl, M.; Junge, H.; Beller, M.; Hollmann, D.; Brückner, A. Water reduction with visible light: Synergy between optical transitions and electron transfer in Au-TiO₂ catalysts visualized by in situ EPR spectroscopy. *Angew. Chem., Int. Ed.* **2013**, *52*, 11420–11424
- (30) Chiesa, M.; Paganini, M. C.; Livraghi, S.; Giamello, E. Charge trapping in TiO₂ polymorphs as seen by Electron Paramagnetic

Resonance spectroscopy. Phys. Chem. Chem. Phys. 2013, 15, 9435-9447.

- (31) Minato, T.; Susaki, T.; Shiraki, S.; Kato, H. S.; Kawai, M.; Aika, K. Investigation of the electronic interaction between TiO₂ (110) surfaces and Au clusters by PES and STM. Surf. Sci. **2004**, 566–568, 1012–1017.
- (32) Siemer, N.; Lüken, A.; Zalibera, M.; Frenzel, J.; Muñoz-Santiburcio, D.; Savitsky, A.; Lubitz, W.; Muhler, M.; Marx, D.; Strunk, J. Atomic-Scale Explanation of O₂ Activation at the Au-TiO₂ Interface. *J. Am. Chem. Soc.* **2018**, *140*, 18082–18092.
- (33) McEntee, M.; Stevanovic, A.; Tang, W.; Neurock, M.; Yates, J. T. Electric field changes on Au nanoparticles on semiconductor supports The molecular voltmeter and other methods to observe adsorbate-induced charge-transfer effects in Au/TiO₂ Nanocatalysts. *J. Am. Chem. Soc.* **2015**, *137*, 1972–1982.
- (34) Chen, M. S.; Goodman, D. W. Catalytically active Au: from nano-particles to ultra-thin films. *Acc. Chem. Res.* **2006**, *39*, 739.
- (35) Yoon, B.; Häkkinen, H.; Landman, U.; Wörz, A. S.; Antonietti, J. M.; Abbet, S.; Judai, K.; Heiz, U. Charging Effects on Bonding and Catalyzed Oxidation of CO on Au₈ Clusters on MgO. *Science* **2005**, 307, 403–407.
- (36) Green, I. X.; Tang, W.; Neurock, M.; Yates, J. T. Spectroscopic observation of dual catalytic sites during oxidation of CO on a Au/ ${\rm TiO_2}$ catalyst. *Science* **2011**, 333, 736–739.
- (37) Green, I. X.; Tang, W.; McEntee, M.; Neurock, M.; Yates, J. T. Inhibition at perimeter sites of Au/TiO₂ oxidation catalyst by reactant oxygen. *J. Am. Chem. Soc.* **2012**, *134*, 12717–12723.
- (38) Rao, R. G.; Blume, R.; Hansen, T. W.; Fuentes, E.; Dreyer, K.; Moldovan, S.; Ersen, O.; Hibbitts, D. D.; Chabal, Y. J.; Schlögl, R.; Tessonnier, J. P. Interfacial charge distributions in carbon-supported palladium catalysts. *Nat. Commun.* 2017, 8, 8.
- (39) Zhang, S.; Plessow, P. N.; Willis, J. J.; Dai, S.; Xu, M.; Graham, G. W.; Cargnello, M.; Abild-Pedersen, F.; Pan, X. Dynamical observation and detailed description of catalysts under strong metal-support interaction. *Nano Lett.* **2016**, *16*, 4528–4534.